LAWRENCE
LIVERMORE
NATIONAL
LABORATORY

LLNL-JRNL-523692

Experimental Observations of Turbulent Mixing due to Kelvin - Helmholtz Instability on the OMEGA Laser Facility

V. A. Smalyuk, H. F. Hansen, O. A. Hurricane, G. Langstaff, D. Martinez, H. -S. Park, K. Raman, B. A. Remington, H. F. Robey, O. Schilling, R. Wallace, Y. Elabz, D. Shvarts, C. De Stefano, R. P. Drake, D. Marion, C. M. Krauland, C. C. Kuranz

January 23, 2012

Physics Plasmas

Disclaimer

Experimental Observations of Turbulent Mixing due to Kelvin–Helmholtz Instability on the OMEGA Laser Facility

(LLNL-JRNL-523692)

V. A. Smalyuk, J. F. Hansen, O. A. Hurricane, G. Langstaff, D. Martinez, H.-S. Park, K. Raman, B. A. Remington, H. F. Robey, O. Schilling, and R. Wallace

Lawrence Livermore National Laboratory, Livermore CA 94551

Y. Elbaz, A. Shimony, and D. Shvarts

Physics Department, Nuclear Research Center Negev; and

Physics Department, Ben-Gurion University, Beer-Sheva, Israel

C. Di Stefano, R. P. Drake, D. Marion, C. M. Krauland, and C. C. Kuranz

Department of Atmospheric, Oceanic, and Space Sciences,

University of Michigan, Ann Arbor MI 48109

ABSTRACT

Shear-flow, Kelvin–Helmholtz (KH) turbulent mixing experiments were performed on the OMEGA Laser Facility [T. R. Boehly *et al.*, Opt. Commun. **133**, 495 (1997)] in which laser-driven shock waves propagated through a low-density plastic foam placed on top of a higher-density plastic foil. The plastic foil was comprised of a thin iodine-doped plastic tracer layer bonded on each side to an undoped density- matched

polyamide-imide plastic. Behind the shock front, lower-density foam plasma flowed over the higher-density plastic plasma, such that the interface between the foam and plastic was KH unstable. The initial perturbations consisted of pre-imposed, sinusoidal 2D perturbations, and broadband 3D perturbations due to surface roughness at the interface between the plastic and foam. KH instability growth was measured using side-on radiography with a point-projection 5-keV vanadium backlighter. Time-integrated images were captured on D-8 x-ray film. Spatial density profiles of iodine-doped plastic mixed with foam were inferred using x-ray radiographs. The mixing layer ensuing from the KH instability with layer width up to ~100 μm was observed at a location ~1 mm behind the shock front. The measured mixing layer width was in good agreement with predictions based on a simple self-similar model of KH instability growth using an estimate of the shear velocity obtained from numerical simulations of the experiments.

I. INTRODUCTION

Kelvin–Helmholtz (KH) instability occurs when a velocity shear (i.e., a velocity difference) exists at the interface between two fluids [1]. If two superposed fluids with densities ρ_1 and ρ_2 move with different velocities, a small sinusoidal perturbation on the surface between these fluids will grow exponentially at early times with a linear growth rate

$$\gamma = \frac{\sqrt{\rho_1 \rho_2}}{\rho_1 + \rho_2} kV , \qquad (1)$$

where V is a relative (constant) velocity between the two fluids at the interface and k is the perturbation wave-number [1-3]. Surface tension effects are assumed to be negligible

in Eq. (1). At the onset of nonlinearity, the perturbations will develop into characteristic vortical structures, which eventually result in material mixing in the turbulent regime at large Reynolds numbers [4,5]. The KH instability is important in inertial confinement fusion (ICF), astrophysics, and in any multifluid hydrodynamic mixing process [4,5]. In ICF, target perturbations grow due to shock-driven Richtmyer–Meshkov (RM) instability and Rayleigh–Taylor (RT) instability during the acceleration and deceleration phases of capsule implosions [4-15]. The RM and RT instabilities amplify initial perturbations (arising from target fabrication, for example) to produce an interface consisting of bubbles of low-density material and spikes of high-density material [4-15]. While thin, dense spikes penetrate through low-density material, small perturbations at the spike surface can grow due to KH instability, resulting in mushroom-like structures developing on the tips of the spikes and mixing of two fluids within the vortex cores [4,5]. While RM and RT instabilities have been extensively studied in laser-driven, high-energy-density (HED) experiments [4-15], only a few experiments have been performed to study the formation and physics of KH instability [16-22]. This is largely due to the much greater difficulty associated with imaging and quantifying KH mixing in HED conditions, unlike in fluid and gas experiments, where experimental methods and techniques are significantly more developed [23-25]. Atomic mixing of heavier ablators with lighter gas fuel was detected in ICF implosions using x-ray spectroscopy [15, 26-28] and nuclear diagnostics [29-35]. The mixing was attributed to unstable perturbation growth due to RM, RT, and KH instabilities, and mixing models were developed to explain the experimental observations [36-39]. However, the understanding of KH instability and

mixing is much less advanced than for RM and RT instabilities which can be imaged more easily in HED conditions.

Only a few dedicated KH experiments were conducted in HED plasmas [16-20]. The initial experiments were inconclusive as to whether the observed growth was actually due to KH instability [16]. Subsequent OMEGA experiments using a new target design with pre-imposed 2D sinusoidal perturbations produced excellent data, showing vortex development due to KH instability [17-20]. The same platform was recently used to study turbulent mixing in HED plasma shear flows [40] and an effort is currently underway to calibrate mix models in the HED regime [41,42]. The present experiments and analysis extend these recent studies [40,42], and examine KH unstable plasma flows emerging from pre-imposed 2D sinusoidal perturbations and 3D broadband perturbations. Compared to previous HED experimental studies of KH instability, the present study presents quantitative evidence of mixing through spatial density profiles of the mixed plasma-state materials.

The experimental configuration is presented in Sec. II. Section III describes the spatial resolution measurements. Section IV presents the results of experiments with 2D initial perturbations. KH mixing experiments and modeling are described in Sec. V. Finally; the results are summarized in Sec. VI.

II. EXPERIMENTAL SETUP

The new experiments used the experimental configuration developed in a previous campaign [18,19]. Figure 1 shows a schematic of the target and experimental configuration. The main target components consisted of carbonized resorcinol

formaldehyde (CRF) foam and a plastic foil with an interface parallel to the direction of shock-wave propagation. The shock wave was initiated by a laser drive using 10 overlapping OMEGA beams [43] with 1-ns square laser pulse shape and peak intensity of ~8×10^{14} W/cm^2. The laser beams in these experiments used smoothing techniques including distributed phase plates (DPPs) [44], polarization smoothing (PS) [45], and smoothing by spectral dispersion (SSD) [46]. A laser-driven shock wave was launched in the 30-μm thick plastic ablator, on the left side of the target shown in Fig 1. The shock propagated through low-density plastic foam placed on a higher-density plastic assembly from left to right. Behind the shock front, lower-density foam plasma flowed over higher-density plastic plasma, rendering the interface between the foam and plastic KH unstable.

A 50-μm thick gold washer (coated with ~20-μm thick plastic) and a 1-mm thick acrylic shield prevented laser light from directly irradiating the plastic target and beryllium shock tube containing the plastic–foam assembly. A gold grid with a 63.5 μm period was used as a fiducial for distance calibration and resolution measurements. Some targets had plastic–foam interfaces with 2D sinusoidal perturbations with wavelengths of 400 μm and initial amplitudes of 30 μm for some experiments, while other targets used flat interfaces, apart from the cellular nature of the foam and surface roughness from machining of the plastic. The surface roughness of the plastic portion of the target ranged from ~50–100 nm with a flat Fourier spectrum. The surface perturbations served as initial 3D perturbations for the turbulent mixing experiments. Three types of foam were used in these experiments with initial densities of 50, 100, and 200 mg/cc. As in previous experiments, the plastic portion of the main target contained a 200-μm wide iodine-doped CH layer. The initial density of iodine-doped (3% atomic) plastic was 1.43 g/cc. Iodine

dopant was used to increase the contrast to 5 keV backlighter x-rays and to preferentially image a central part of the target. Vanadium point projection backlighting was used to image perturbation growth with D-8 x-ray film as a detector [18,19]. The film was digitized with a square aperture of 22 × 22 μm. See Fig. 2 in References [18,19] for additional details of the target geometry.

An example of the data with 100 mg/cc foam taken at 75 ns after the beginning of the drive is shown in Fig. 2. The ablator of the target was directly driven with laser light, producing a strong shock that propagated through the target from left to right with speed of ~60 μm/ns. The shock produced a velocity difference at the interface between the foam and plastic, resulting in KH instability growth of the pre-imposed perturbation. As the shock travelled from right left, the perturbations near the left part of the image had more time to grow than those near the right part. The lighter color in the image corresponds to more-transparent foam, while the darker color corresponds to more opaque plastic. The initial 2D sinusoidal, 400-μm-wavelength perturbation developed into vortices. In addition, the growth of small-scale perturbations due to 3D surface imperfections resulted in the “hair-like” non-uniformities that can be seen around the 2D vortices. These non-uniformities represent turbulent mixing of two materials, as expected since the Reynolds number was large in this experiment, $Re \sim 1 \times 10^6$, and the evolution time of the experiment was on the order of a few vortex turnover times. [18] The quantitative description of the mixing layer evolution is the principal focus of this study. The growth of sinusoidal 2D perturbations was used primarily to validate code predictions, as the simulated interface flow velocity was used in a mixing model to compare with measured mix profiles.

III. SPATIAL RESOLUTION MEASUREMENTS

The spatial resolution and magnification of the system was characterized by a gold fiducial grid in each shot. An example of a grid image is shown in Fig. 2. The nominal distance between the backlighter and the target was ~1 mm, while the distance between the target and the detector was ~230 mm, resulting in a nominal magnification of ~24 in these experiments. Figure 3 describes details of the spatial resolution measurements performed using the Au grid. The square structure in Fig. 3(a) represents intensity distribution at the grid without blurring due finite spatial resolution. The thin solid line in Fig. 3(a) represents the measured light intensity blurred by the imaging system, and the thick solid line is the fit to experimental data assuming that the system modulation transfer function (MTF) is a bi-Gaussian function [47] shown in Fig. 3(b). The inferred spatial resolution was ~17 μm, and the magnification was ~26 for this measurement. The measured magnification, inferred from the grid images, varied between 22 and 26 due to variations of grid position with respect to the main target, the spatial resolution was the same from shot to shot. The measured spatial resolution was slightly better than the 20 μm diameter pinhole used in these point-projection backlighting experiments. The pinhole closes slightly due to ablation caused by the backlighter beams during the 1-ns drive, slightly improving the spatial resolution. This was consistent with previous similar experiments [18,19].

IV. KELVIN–HELMHOLTZ INSTABILITY EXPERIMENTS WITH 2D PERTURBATIONS

Figure 2 shows the presence of “hair-like” structures in addition to the KH vortices developing from the initial 2D sinusoidal, 400-μm-wavelength perturbations. This is a new observation, compared to data from previous experiments with nominally the same targets [18]. The presence of such 3D structures can be attributed to the difference in initial conditions: the surface roughness in either the plastic or foam was different compared to that of previous experiments. The evolution of 2D vortices was very similar in both sets of experiments. The shot shown in Fig. 2 was repeated with the same drive conditions using 100 mg/cc foam. Figure 4 shows that turbulent “hair-like” structures were reproducible in a recent campaign. The density of foam material was also varied in several subsequent shots. Figure 5 shows images with 50, 100, and 200 mg/cc foam taken at 47, 75, and 119 ns. Based on 2D simulations [18], the timing of these experiments was chosen to allow the same KH growth for all three types of foam, with the lower density foam target evolving more quickly and the higher density foam target evolving more slowly than the nominal 100 mg/cc target. Again, all shots revealed the presence of turbulent structures regardless of the type of foam.

A comparison with 2D simulation is shown in Fig. 5 for the shot with 100 mg/cc foam at 75 ns. The simulation was post-processed to include the effects of spatial resolution, and absorption of foam and plastic. In these new experiments, the vortices in the 2D simulations are larger than in the experiment, consistent with previous results. It is now understood that 3D effects in the drive and 3D expansion of the shock tube reduced late-time vortex amplitudes in the experiment compared to simulations [18,19]. This 3D

effect was noticeable after 35 ns from the beginning of the drive, while 2D vortices in the simulations and experiments were similar before 35 ns [19]. Additionally, synthetic radiographs from simulations do not show absorption near the vortex stems or turbulent structures above the vortices.

Again, the presence of turbulent mixing was expected based on the large predicted Reynolds number, Re ~ 1×10^6, and relatively long evolution time allowed by the experimental platform [18]. Based on a comparison between the previous and new campaigns, it is suggested that turbulent, “hair-like” structures appear earlier in time in the new experiments, possibly due to increased surface roughness at the plastic or foam surfaces. While the appearance of the small-scale structures can be attributed to the increased surface roughness, it should be noted that the "hair-like" structure, in contrast to the more familiar "vortex" structure is a known feature of high Atwood number shear flow instability. This feature was observed in numerical simulations of multimode Kelvin-Helmholtz instability by Rikanati, Alon, and Shvarts [48]. Images with 50 mg/cc foam have more “hair-like” structures than with 200 mg/cc foam, as expected, because Atwood number is higher in 50 mg/cc foam.

Figure 7 shows three measured density profiles as a function of distance in the vertical direction above the three vortices, as indicated by the arrows in Fig. 6(b). The density was inferred using the optical depth (OD) of the backlighter absorption in the iodine-doped CH (CHI), mass absorption coefficient at backlighter x-ray energy of 5 keV, and the length of CHI region, 200 μm. The measured OD is proportional to the target areal density [$\rho R(t)$], [OD(t)] = $\mu_{\mathrm{CHI}}(E)$[$\rho R(t)$], where $\mu_{\mathrm{CHI}}(E)$ is the CHI mass-absorption rate, and t is the time of the measurement. The CHI density in the mixed

region is obtained by dividing the target areal density by the width of the CHI region R = 200 μm, $\rho(t) = [\rho R(t)] / R$. The contributions of the foam and plastic materials around the CHI to the total measured OD were negligible at the backlighter x-ray energy. The zero location of the distance axis in Fig. 7 corresponds to the minimum of x-ray transmission along the arrows in Fig. 6(b). The density of CHI decreased exponentially away from the vortices. This experimental method was sensitive to detecting mixing of CHI with smallest density of ~0.01 g/cc, or approximately 100 times below the initial uncompressed CHI density of 1.43 g/cc. The extent of mixing was increasing in time, as there was a larger extent of the mixing (~100 μm) above the vortices on the left-hand side compared to right-hand side. Expected molecular diffusion scale was ~0.04 microns, as calculated based on predicted plasma conditions at ~30-100 ns after the start of the drive, therefore, the molecular diffusion had negligible contribution to the measured mixing width.

V. KELVIN–HELMHOLTZ INSTABILITY EXPERIMENTS WITH 3D PERTURBATIONS

As the presence of large 2D perturbations can affect the interpretation of the 3D turbulent mixing, additional experiments were performed with nominally unperturbed interfaces, in which the KH growth can occur only due to 3D surface roughness. Figure 8 shows the KH growth image with 100 mg/cc foam measured at 35 ns. As mentioned above, 2D simulations showed good agreement with measurements before 35 ns [18]. Therefore, code predictions for the interface velocity can be used in a mixing model to compare with the experimentally measured mixing width. Positions of the shock front,

mixing layer, and spatial distances behind the shock front are also identified in the image. Figure 9 shows the spatial extent of the mixed CHI in the foam in the vertical direction away from the plastic–foam interface, at locations ranging from 0 to 700 μm behind the shock front. The measured image was at 35 ns after the beginning of the drive. The zero location of the distance axis in Fig. 9 corresponds to the minimum of x-ray transmission, similar to Fig.7. The spatial extent of mixing is increasing with the distance behind the shock front. The density of mixed CHI decreases exponentially in the foam material, away from the plastic–foam interface.

Figure 10 shows the dynamics of the shear velocity between the foam and plastic materials, as predicted by numerical simulations. Immediately after the passage of the shock, the shear velocity spikes at ~45 μm/ns, sharply decreases to ~15 μm/ns before ~40 ns, and then gradually deceases to zero up to ~100 ns. This evolution corresponds to a spatial location shown by the arrow at 1000 μm in the image on Fig. 8. Therefore, the largest KH growth is experienced during the first ~40 ns after the passage of the shock wave.

The measured extent of the mixing was compared with the prediction of a self-similar mixing model [21]. Self-similarity of the later time KH growth was expected based on experimental KH data from shock tube experiments with liquids and gases [23, 24, 48]. The model predicts that the mixing width $w(t)$ increases with time t in a very large Reynolds number self-similar regime, and is proportional to the interface velocity V: $w(t) = \delta V t$, where $\delta \approx 0.18$ is a constant derived from classical fluid dynamics experiments [23, 49]. This expression follows from dimensional considerations, in which the only length-scale that can be formed from the available dimensional quantities V and t

is proportional to $V\,t$. As the interface velocity varies in time in the present experiments, the mixing width definition was generalized to

$$w(t) = \delta \int_0^t V(t')\, dt' . \qquad (2)$$

Note that the value $\delta = 0.18$ is adopted here, although there is no a priori justification for assuming that it has the same value as determined in incompressible fluid experiments; the flow of the neutral foam and plastic plasmas is assumed to be incompressible. The generalization of the self-similar mixing layer width to a time-dependent relative velocity $V(t)$, Eq. (2), is analogous to the generalization to a time-dependent acceleration in self-similar Rayleigh–Taylor instability growth: $w(t) = \alpha\, A \int_0^t \int_0^{t'} g(t'')dt''dt'$, where α is a dimensionless self-similar growth parameter and A is the Atwood number, or $w(t) = \alpha A \left[\int_0^t \sqrt{g(t')}dt' \right]^2$ [50, 51].

The predictions of the simple self-similar mixing model provide less-detailed information than the experiments do. Detailed spatial profiles of the mixed material are measured in the experiments, while in the model the mixing layer width is represented by a single number $w(t)$ at a given time. Figure 11 shows the evolution of the calculated mixing layer width by a thick solid curve based on Eq. (2) and the simulated interface velocity as a function of distance behind the shock front at 35 ns after the beginning of the drive. The squares, triangles, and diamonds correspond to the mixing layer widths calculated from the experimental data at CHI density profiles of 0.1, 0.03 and 0.01 g/cc,

respectively. The predicted width agrees with the experimentally measured width at a density profile between 0.1 and 0.03 g/cc.

While the present experiments were characterized by high Atwood numbers (A~0.7-0.8), the coefficient $\delta \approx 0.18$ was derived from classical fluid dynamics experiments [23, 49] with A=0, as discussed above. It was assumed the total mixing width (i.e. the 0.18 coefficient) doesn't depend on the Atwood number but the asymmetry of penetration to both material does, increasing the penetration of the heavy material to the light material (in the form of "hairs" or "spikes") while decreasing the light material penetration into the heavy material. Therefore, the problem of definition of the total mixing width is more dependent on the definition of the heavy material penetration than the light to heavy one. As was shown above, for the experiments discussed in this study a value between 0.03-0.1 g/cc gives good agreement to a simple mix model but we suggest to refine the mixing width definition in a future work, using insight from full numerical simulations.

Simple asymptotic models based on self-similarity of the unstable RT, RM, and KH growth in the highly nonlinear, turbulent regime do not include a dependence on initial conditions [21]. The experiments presented here indicate the importance of initial conditions to the growth in the turbulent regime based on two sets of experimental data. Future experiments will study the dependence of KH growth from initial conditions by systematically varying the initial perturbations.

VI. CONCLUSION

Kelvin–Helmholtz (KH) instability experiments were performed on the OMEGA Laser Facility to study turbulent mixing in high-energy-density plasmas with large Reynolds numbers, Re ~ 1×10^6. Laser-driven shock waves propagated through low-density plastic foam placed on top of higher-density plastic foils. Behind the shock front, lower-density foam plasma flowed over higher-density plastic plasma, resulting in a KH unstable interface between the foam and plastic. Penetration of the heavier plastic plasma into the lighter foam plasma was measured using side-on x-ray radiography. Density profiles of mixed plastic were inferred from measured x-ray images. Measurements were performed with foam–plastic interfaces having pre-imposed 2D, sinusoidal perturbations, and flat interfaces with surface roughness having rms of ~100 nm. In both types of targets, penetration of the plastic into the foam was observed with the formation of turbulent, "hair-like" structures. The plastic extended approximately 100 μm into the foam after ~35 ns of the KH instability growth, with the plastic density falling approximately exponentially away from the plastic–foam interface. The experimental mixing layer growth was compared with predictions of a self-similar mixing model based on the interface velocity derived from 2D simulations. The predicted mixing width agrees with the measured width at plastic density profiles of approximately 0.03–0.1 g/cc, or ~30 times lower than the initial plastic density. The experiments presented here indicate the importance of initial conditions to the growth in the turbulent regime based on two sets of experimental data. Future experiments will investigate the dependence of KH mixing in HED plasmas on the initial conditions.

ACKNOWLEDGMENT

This work was performed under the auspices of the U.S. Department of Energy by Lawrence Livermore National Laboratory under Contract DE-AC52-07NA27344. The contributions by the University of Michigan were funded by the NNSA-DS and SC-OFES Joint Program in High-Energy-Density Laboratory Plasmas, by the National Laser User Facility Program in NNSA-DS and by the Predictive Sciences Academic Alliances Program in NNSA-ASC. The corresponding grant numbers are DE-FG52-09NA29548, DE-FG52-09NA29034, and DE-FC52-08NA28616.

REFERENCES

[1] L. D. Landau and E. M. Lifshitz, *Fluid Mechanics* (Pergamon Press, London, 1958) p. 114.

[2] S. Chandrasekhar, *Hydrodynamic and Hydromagnetic Stability* (Dover, Mineola, New York, 1961).

[3] P. G. Drazin and W. H. Reid, *Hydrodynamic Stability*, second edition (Cambridge University Press, Cambridge, UK, 2004).

[4] J. D. Lindl, *Inertial Confinement Fusion: The Quest for Ignition and Energy Gain Using Indirect Drive* (Springer-Verlag, New York, 1998).

[5] S. Atzeni and J. Meyer-ter-Vehn, *The Physics of Inertial Fusion: Beam Plasma Interaction, Hydrodynamics, Hot Dense Matter*, International Series of Monographs on Physics (Clarendon Press, Oxford, 2004).

[6] Lord Rayleigh, Proc. London Math Soc. **XIV**, 170 (1883).

[7] G. Taylor, Proc. R. Soc. London Ser. A **201**, 192 (1950).

[8] J. Nuckolls, L. Wood, A. Thiessen, and G. Zimmerman, Nature **239**, 139 (1972).

[9] S. E. Bodner, D. G. Colombant, J. H. Gardner, R. H. Lehmberg, S. P. Obenschain, L. Phillips, A. J. Schmitt, J. D. Sethian, R. L. McCrory, W. Seka, C. P. Verdon, J. P. Knauer, B. B. Afeyan, and H. T. Powell, Phys. Plasmas **5**, 1901 (1998).

[10] B. A. Remington, S. V. Weber, S. W. Haan, J. D. Kilkenny, S. G. Glendinning, R. J. Wallace, W. H. Goldstein, B. G. Wilson, and J. K. Nash, Phys. Fluids B **5**, 2589 (1993).

[11] B. A. Remington, S. V. Weber, M. M. Marinak, S. W. Haan, J. D. Kilkenny, R. Wallace, and G. Dimonte, Phys. Rev. Lett. **73**, 545 (1994).

[12] B. A. Remington, J. Kane, R. P. Drake, S. G. Glendinning, K. Estabrook, R. London, J. Castor, R. J. Wallace, D. Arnett, E. Liang, R. McCray, A. Rubenchik, and B. Fryxell, Phys. Plasmas **4**, 1994 (1997).

[13] V. A. Smalyuk, O. Sadot, J. A. Delettrez, D. D. Meyerhofer, S. P. Regan, and T. C. Sangster, Phys. Rev. Lett. **95**, 215001 (2005).

[14] C. W. Barnes, S. H. Batha, A. M. Dunne, G. R. Magelssen, S. Rothman, R. D. Day, N. E. Elliott, D. A. Haynes, R. L. Holmes, J. M. Scott, D. L. Tubbs, D. L. Youngs, T. R. Boehly, and P. A. Jaanimagi, Phys. Plasmas **9**, 4431 (2002).

[15] V. A. Smalyuk, V. N. Goncharov, J. A. Delettrez, F. J. Marshall, D. D. Meyerhofer, S. P. Regan, and B. Yaakobi, Phys. Rev. Lett. **87**, 155002 (2001).

[16] B. A. Hammel, J. D. Kilkenny, D. Munro, B. A. Remington, H. N. Kornblum, T. S. Perry, D. W. Phillion, and R. J. Wallace, Phys. Plasmas **1**, 1662 (1994).

[17] O. A. Hurricane, High Energy Density Phys. **4**, 97 (2008).

[18] O. A. Hurricane, J. F. Hansen, H. F. Robey, B. A. Remington, M. J. Bono, E. C. Harding, R. P. Drake, and C. C. Kuranz, Phys. Plasmas **16** 056305 (2009).

[19] E. C. Harding, J. F. Hansen, O. A. Hurricane, R. P. Drake, H. F. Robey, C. C. Kuranz, B. A. Remington, M. J. Bono, M. J. Grosskopf, and R. S. Gillespie, Phys. Rev. Lett. **103** 045005 (2009).

[20] O. A. Hurricane, J. F. Hansen, E. C. Harding, V. A. Smalyuk, B. A. Remington, G. Langstaff, H.-S. Park, H. F. Robey, C. C. Kuranz, M. J. Grosskopf, and R. S. Gillespie, Astrophys. Space Sci. **336**, 139 (2011).

[21] E. C. Harding, R. P. Drake, R. S. Gillespie, M. J. Grosskopf, A. Visco, J. Ditmar, Y. Aglitskiy, J. L. Weaver, A. L. Velikovich, "Laser driven supersonic flow over a compressible foam surface on the Nike laser," Phys. Plasmas, in press.

[22] E. C. Harding, R. P. Drake, R. S. Gillespie, M. J. Grosskopf, A. Visco, J. Ditmar, Y. Aglitskiy, J. L. Weaver, A. L. Velikovich, "Experimental design to generate strong shear layers in a high-energy-density plasma," High Energy Density Phys., in press.

[23] P. E. Dimotakis, *Turbulent Free Shear Layer Mixing and Combustion*, High-Speed Flight Propulsion Systems, Progress in Aeronautics and Astronautics Vol. **137**, edited by S. N. B. Murthy and E. T. Curran, pp. 265-340. (1991).

[24] P. E. Dimotakis, *On the Convection Velocity of Turbulent Structures in Supersonic Shear Layers*, AIAA Paper 91-1724 (1991).

[25] Y. Zhou, Phys. Plasmas **14**, 082701 (2007).

[26] T. R. Dittrich, B. A. Hammel, C. J. Keane, R. McEachern, R. E. Turner, S. W. Haan, and L. J. Suter, Phys. Rev. Lett. **73**, 2324 (1994).

[27] S. P. Regan, J. A. Delettrez, F. J. Marshall, J. M. Soures, V. A. Smalyuk, B. Yaakobi, V. Yu. Glebov, P. A. Jaanimagi, D. D. Meyerhofer, P. B. Radha, W. Seka, S. Skupsky, C. Stoeckl, R. P. J. Town, D. A. Haynes, Jr., I. E. Golovkin, C.

F. Hooper, Jr., J. A. Frenje, C. K. Li, R. D. Petrasso, and F. H. Séguin, Phys. Rev. Lett. **89**, 085003 (2002).

[28] B. Yaakobi, V. A. Smalyuk, J. A. Delettrez, F. J. Marshall, D. D. Meyerhofer, and W. Seka, Phys. Plasmas **7**, 3727 (2000).

[29] M. D. Cable, S. P. Hatchett, J. A. Caird, J. D. Kilkenny, H. N. Kornblum, S. M. Lane, C. Laumann, R. A. Lerche, T. J. Murphy, J. Murray, M. B. Nelson, D. W. Phillion, H. Powell, and D. B. Ress, Phys. Rev. Lett. **73**, 2316 (1994).

[30] D. D. Meyerhofer, J. A. Delettrez, R. Epstein, V. Yu. Glebov, V. N. Goncharov, R. L. Keck, R. L. McCrory, P. W. McKenty, F. J. Marshall, P. B. Radha, S. P. Regan, S. Roberts, W. Seka, S. Skupsky, V. A. Smalyuk, C. Sorce, C. Stoeckl, J. M. Soures, R. P. J. Town, B. Yaakobi, J. D. Zuegel, J. Frenje, C. K. Li, R. D. Petrasso, D. G. Hicks, F. H. Séguin, K. Fletcher, S. Padalino, M. R. Freeman, N. Izumi, R. Lerche, T. W. Phillips, and T. C. Sangster, Phys. Plasmas **8**, 2251 (2001).

[31] P. B. Radha, J. Delettrez, R. Epstein, V. Yu. Glebov, R. Keck, R. L. McCrory, P. McKenty, D. D. Meyerhofer, F. Marshall, S. P. Regan, S. Roberts, T. C. Sangster, W. Seka, S. Skupsky, V. Smalyuk, C. Sorce, C. Stoeckl, J. Soures, R. P. J. Town, B. Yaakobi, J. Frenje, C. K. Li, R. Petrasso, F. Séguin, K. Fletcher, S. Padalino, C. Freeman, N. Izumi, R. Lerche, and T. W. Phillips, Phys. Plasmas **9**, 2208 (2002).

[32] C. K. Li, F. H. Séguin, J. A. Frenje, S. Kurebayashi, R. D. Petrasso, D. D. Meyerhofer, J. M. Soures, J. A. Delettrez, V. Yu. Glebov, P. B. Radha, F. J.

Marshall, S. P. Regan, S. Roberts, T. C. Sangster, and C. Stoeckl, Phys. Rev. Lett. **89**, 165002 (2002).

[33] J. R. Rygg, J. A. Frenje, C. K. Li, F. H. Séguin, R. D. Petrasso, V. Yu. Glebov, D. D. Meyerhofer, T. C. Sangster, and C. Stoeckl, Phys. Rev. Lett. **98**, 215002 (2007).

[34] J. R. Rygg, J. A. Frenje, C. K. Li, F. H. Séguin, R. D. Petrasso, J. A. Delettrez, V. Yu. Glebov, V. N. Goncharov, D. D. Meyerhofer, P. B. Radha, S. P. Regan, and T. C. Sangster, Phys. Plasmas **14**, 056306 (2007).

[35] D. C. Wilson, P. S. Ebey, T. C. Sangster, W. T. Shmayda, V. Yu. Glebov, and R. A. Lerche, Phys. Plasmas **18**, 112707 (2011).

[36] A. J. Scannapieco and B. Cheng, Phys. Lett. A **299**, 46 (2002).

[37] D. C. Wilson, A. J. Scannapieco, C. W. Cranfill, M. R. Clover, N. M. Hoffman, and J. Collins, Phys. Plasmas **10**, 4427 (2003).

[38] G. Dimonte and R. Tipton, Phys. Fluids **18**, 085101 (2006).

[39] D. C. Besnard, F. H. Harlow, R. M. Rauenzahn, and C. Zemach, Theor. Comput. Fluid Dyn. **8**, 1 (1996).

[40] V. A. Smalyuk, H. F. Hansen, O. A. Hurricane, D. Martinez, H.-S. Park, K. Raman, B. A. Remington, H. F. Robey, O. Schilling, R. Wallace, Y. Elbaz, D. Shvarts, C. Di Stefano, R. P. Drake, D. Marion, C. M. Krauland, and C. C. Kuranz, "Measurements of turbulent Kelvin-Helmholtz growth in planar targets on OMEGA," Bull. Am. Phys. Soc. **53**, 179 (2011).

[41] P. Keiter, J. Fincke, L. Welser-Sherill, E. Loomis, and D. Offerman, "Preliminary results from a shear-driven mix experiment," Bull. Am. Phys. Soc. **53**, 179 (2011).

[42] O. A. Hurricane, V. A. Smalyuk, K. Raman, H.F. Hansen, G. Langstaff, D. Martinez, H.-S. Park, B. A. Remington, H. F. Robey, O. Schilling, R. Wallace, C. Di Stefano, R. P. Drake, D. Marion, C. M. Krauland, and C. C. Kuranz, "*Model Validation of Turbulently Mixed Kelvin-Helmholtz Shear Layers using a High Energy Density OMEGA Experiment*," submitted to Physical Review Letters.

[43] T. R. Boehly, D. L. Brown, R. S. Craxton, R. L. Keck, J. P. Knauer, J. H. Kelly, T. J. Kessler, S. A. Kumpan, S. J. Loucks, S. A. Letzring, F. J. Marshall, R. L. McCrory, S. F. B. Morse, W. Seka, J. M. Soures, and C. P. Verdon, Opt. Commun. **133**, 495 (1997).

[44] Y. Lin, T. J. Kessler, and G. N. Lawrence, Opt. Lett. **20**, 764 (1995).

[45] T. R. Boehly, V. A. Smalyuk, D. D. Meyerhofer, J. P. Knauer, D. K. Bradley, R. S. Craxton, M. J. Guardalben, S. Skupsky, and T. J. Kessler, J. Appl. Phys. **85**, 3444 (1999).

[46] S. P. Regan, J. A. Marozas, J. H. Kelly, T. R. Boehly, W. R. Donaldson, P. A. Jaanimagi, R. L. Keck, T. J. Kessler, D. D. Meyerhofer, W. Seka, S. Skupsky, and V. A. Smalyuk, J. Opt. Soc. Am. B **17**, 1483 (2000).

[47] V. A. Smalyuk, T. R. Boehly, L. S. Iwan, T. J. Kessler, J. P. Knauer, F. J. Marshall, D. D. Meyerhofer, C. Stoeckl, B. Yaakobi, and D. K. Bradley, Rev. Sci. Instrum. **72**, 635 (2001).

[48] A. Rikanati, U. Alon, and D. Shvarts, Phys. Fluids **15**, 3776 (2003).

[49] N. Rajaratnam, *Turbulent Jets* (Elsevier, Amsterdam, 1976).

[50] N. N. Anuchina, Yu. A. Kucherenko, V. E. Neuvazhaev, V. N. Ogibina, L. I. Shibarshov and V. G. Yakovlev, Fluid Dynamics **6**, 916 (1978).

[51] D. L. Youngs, Physica D **12**, 32 (1984).

FIGURE CAPTIONS

FIG. 1 (Color online). Experimental configuration and schematic of the target. The shock wave propagates from left to right. (Image taken from Ref. [19]).

FIG. 2. An example of the data with 100 mg/cc foam measured at 75 ns after the beginning of the drive. As the shock travelled from right to left, the vortices at the left part of the image had more time to grow than the perturbations at the right part. The lighter color in the image corresponds to low optical depth (foam plus Be), while the darker color to high optical depth (the iodine-doped plastic).

FIG. 3. (a) The thin solid line is the measured light intensity blurred by the imaging system, and the thick solid line is the fit to experimental data based on the (b) modulation transfer function (MTF) as a function of spatial frequency.

FIG. 4. Reproducibility of turbulent “hair-like” structures is shown by the comparison of two shots (a) and (b) with 100 mg/cc foam taken at 75 ns after the beginning of the drive.

FIG. 5. Measured image with (a) 50 mg/cc foam taken at 47 ns, (b) 100 mg/cc foam at 75 ns, and (c) 200 mg/cc foam at 119 ns after the beginning of the drive. Turbulent “hair-like” structures are present in all images with various foam densities.

FIG. 6. (a) Simulated and (b) measured radiographs of the experiment with 100 mg/cc foam taken at 75 ns after the beginning of the drive. The arrows represent locations of the mixed CHI spatial profiles presented in Fig. 7.

FIG. 7. Spatial density profiles of the mixed CHI in foam are shown at locations represented by arrows in Fig. 6.

FIG. 8. Measured radiograph of the experiment with flat interface using 100 mg/cc foam taken at 75 ns after the beginning of the drive. Positions of the shock front and mixed regions are indicated with arrows. A slightly light feature at the bottom of the image is due to a light leak in the diagnostic.

FIG. 9. Spatial density profiles of the mixed CHI in a foam at locations of 0, 100, 300, 500, and 700 μm behind the shock front measured at 35 ns after the beginning of the drive in the experiment with 100 mg/cc foam.

FIG. 10. Simulated shear velocity as a function of time for the location of 1000 μm behind the shock front, as shown by the arrow in Fig. 8.

FIG. 11. Mixing layer width as a function of position behind the shock front predicted by the self-similar mixing model (thick solid curve) and measured at density profiles of 0.1 (squares), 0.03 (triangles) and 0.01 g/cc (diamonds) at 35 ns.

Figure 1

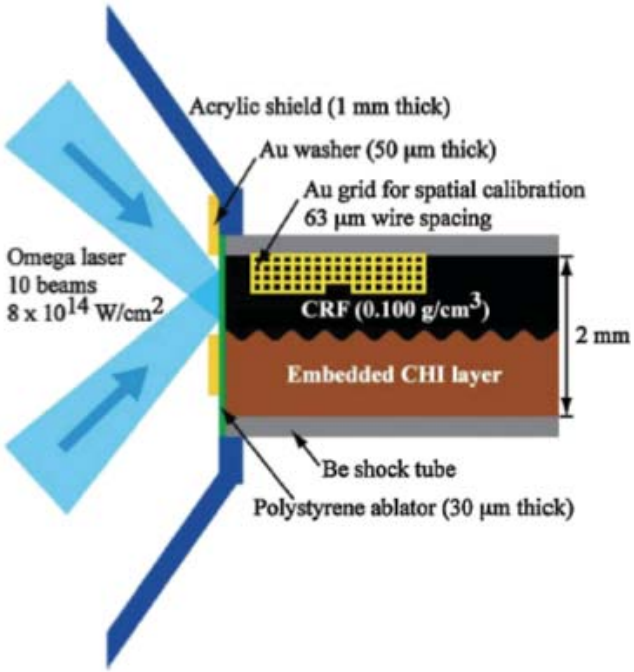
Acrylic shield (1 mm thick)
Au washer (50 μm thick)
Au grid for spatial calibration
63 μm wire spacing
Omega laser
10 beams
8 x 10^14 W/cm^2
CRF (0.100 g/cm^3)
2 mm
Embedded CHI layer
Be shock tube
Polystyrene ablator (30 μm thick)

Figure 2

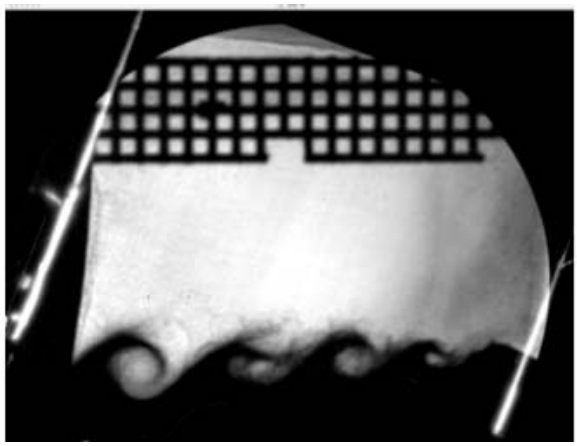

Figure 3

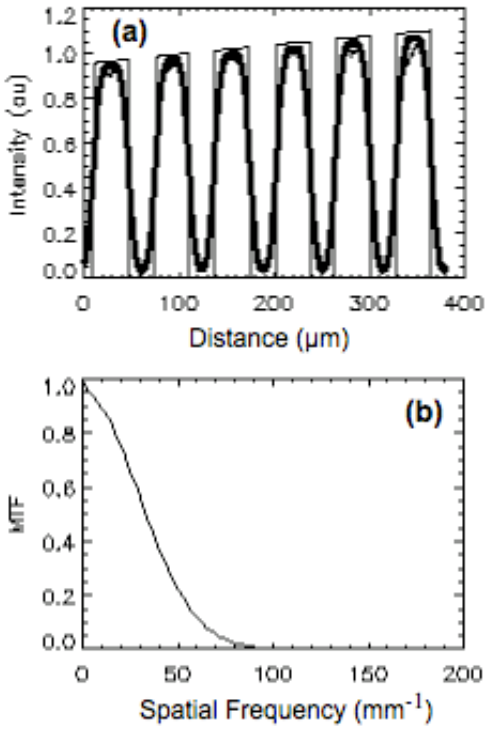
(a)
Intensity (au)
1.2
1.0
0.8
0.6
0.4
0.2
0.0
0
100
200
300
400
Distance (μm)
(b)
MTF
1.0
0.8
0.6
0.4
0.2
0.0
0
50
100
150
200
Spatial Frequency (mm-1)

Figure 4

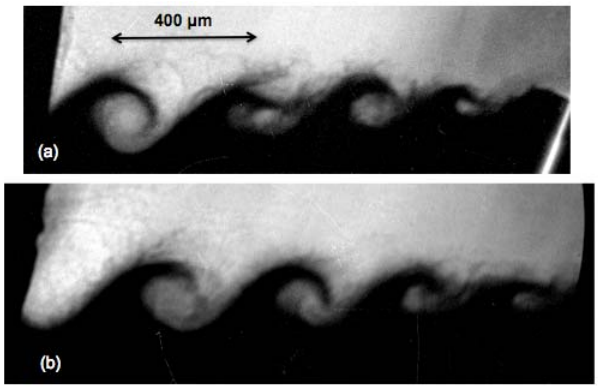

Figure 5

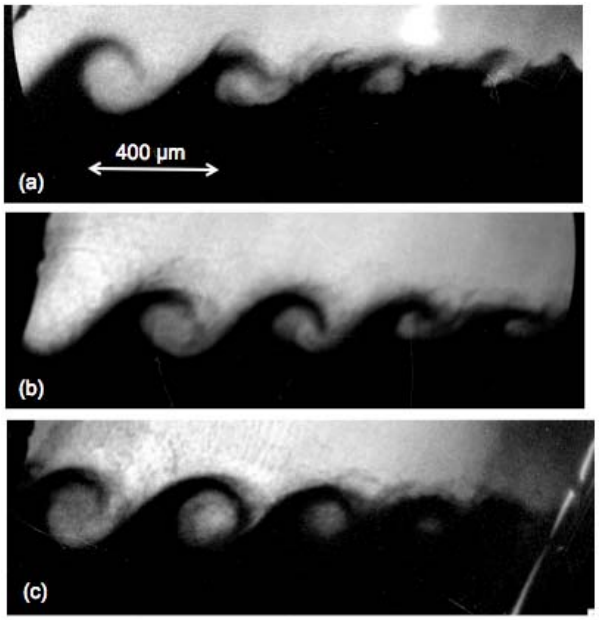

Figure 6

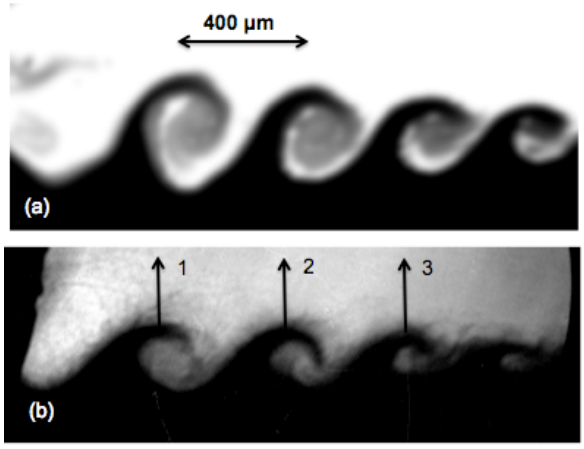

Figure 7

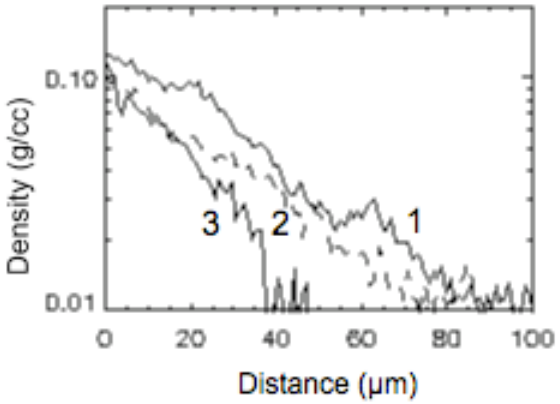

Figure 8

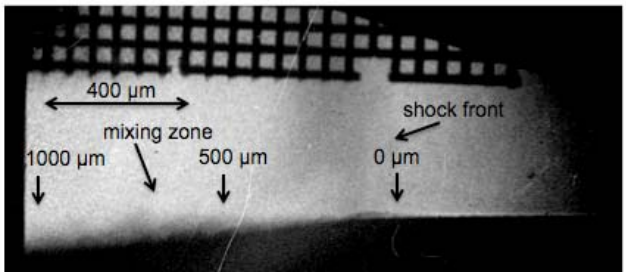

Figure 9

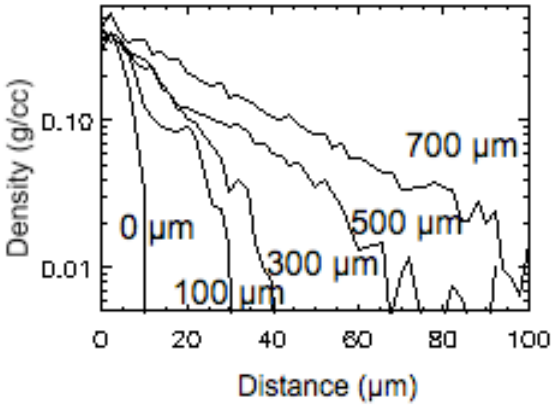
Density (g/cc)
0.10
0.01
0 µm
100 µm
300 µm
500 µm
700 µm
0
20
40
60
80
100
Distance (µm)

Figure 10

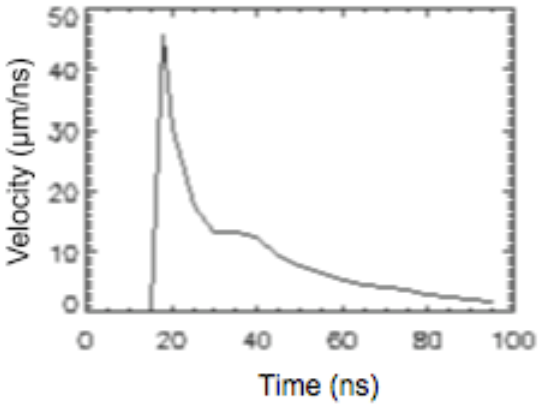

Figure 11